Elastic Scattering of 150-Mev Negative Pions by Nuclei*†

TADAO A. FUJII
The Enrico Fermi Institute for Nuclear Studies, The University of Chicago, Chicago, Illinois
(Received September 2, 1958)

The elastic scattering of 150-Mev negative pions by complex nuclei was experimentally studied by the use of energy-sensitive Čerenkov detectors with a pulse-height analyzer. The elastic scattering could be distinguished from inelastic processes within the 10-Mev resolution width of these detectors. The differential cross sections of carbon, aluminum, copper, and lead were measured at angles between 18.5° and 43.6°. In addition, measurements on carbon and lead were extended to large angles between 45° and 139°.

It was found that elastic scattering was confined predominantly to the forward angles less than 60°. Calculations based on the optical model with a square well were carried out to obtain the values of parameters which provided the best fit to the data. They are -30 Mev$\geq V_R \geq -40$ Mev, -65 Mev$\geq V_I \geq -75$ Mev, and $1.3\times10^{-13}A^{\frac{1}{3}}$ cm$\leq R \leq 1.4\times10^{-13}A^{\frac{1}{3}}$ cm, where V_R and V_I are real and imaginary parts of the potential, R is the nuclear radius, and A is the nuclear mass. The corresponding values of the reaction mean free path were of the order of the pion Compton wavelength. These values are close to those predicted by Frank, Gammel, and Watson from the knowledge of the pion-nucleon interaction.

I. INTRODUCTION

THE scattering of pions from complex nuclei has been described in terms of the optical model.[1] According to this model, the interaction between pions and nuclei is represented by a complex potential in a wave equation, from which the angular distribution of the elastic scattering and the total cross section for the absorption and inelastic processes can be calculated.

The knowledge of the elementary pion-nucleon interaction has become sufficiently extensive so that theoretical accounts for the optical model potential based on this might be possible.[2] In particular, Frank, Gammel, and Watson[3] have evaluated both real and imaginary parts of the potential from the knowledge of pion-nucleon scattering and also of the capture process $\pi^-+d=n+n$ for the pion energy range below 300 Mev. The present experiment was undertaken to see to what extent such calculations could be made to fit the observation of the elastic scattering at 150 Mev.

Earlier studies of the elastic scattering from various nuclei have been carried out in detail at 80 Mev by the Columbia group using scintillation counters and a copper absorber.[4] A number of cloud chamber experiments have yielded information on the elastic scattering distribution as a part of their results. Such experiments have been done at 48 Mev for carbon by Shapiro,[5] at 62 Mev for carbon and at 125 Mev for carbon and lead by Lederman *et al.*,[6] and at 230 Mev for carbon and at 250 Mev for lead by Dzhelepov *et al.*[7] The present work, using energy-sensitive Čerenkov detectors and a pulse-height analyzer, complements the elastic scattering data at the energy where the effect of the 180-Mev resonance in pion-nucleon interaction can be expected. The experiments may serve as one of the tests for the assumption that the two-body pion-nucleon force is not appreciably modified inside the nucleus.[2,3]

II. ARRANGEMENT

The experimental arrangement was essentially the same as that used in the work on inelastic scattering of pions by carbon and lead by Miller.[8] The general layout of the experiment is illustrated in Fig. 1. Negative pions emerging from a beryllium target inside the

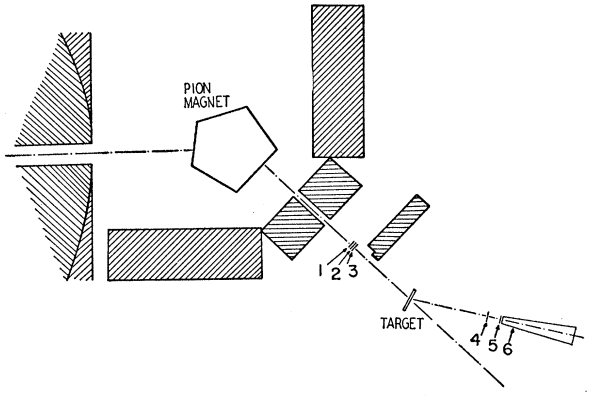

FIG. 1. Experimental arrangement. The monitoring counters are 1, 2, and 3. The gating counters are 4 and 5. The Lucite counter is 6. The shielding is shaded. The target is oriented to be normal to the bisector of the scattering angle.

* Research supported by a joint program of the Office of Naval Research and the U. S. Atomic Energy Commission.

† A thesis submitted to the Department of Physics, the University of Chicago, in partial fulfillment of the requirements for the Ph.D. degree.

[1] S. Lindenbaum, *Annual Review of Nuclear Science* (Annual Reviews, Inc., Palo Alto, 1957), Vol. 7, p. 317; a review article on pion-nucleus scattering.

[2] R. Jastrow, Phys. Rev. **82**, 261 (1951); K. M. Watson, Phys. Rev. **89**, 575 (1953); N. C. Francis and K. M. Watson, Phys. Rev. **92**, 291 (1953); R. M. Sternheimer, Phys. Rev. **101**, 384 (1956).

[3] Frank, Gammel, and Watson, Phys. Rev. **101**, 891 (1956).

[4] Isaacs, Sachs, and Steinberger, Phys. Rev. **85**, 718 (1952); Pevsner, Rainwater, Williams, and Lindenbaum, Phys. Rev. **100**, 1419 (1955); Williams, Rainwater, and Pevsner, Phys. Rev. **101**, 412 (1956); Williams, Baker, and Rainwater, Phys. Rev. **104**, 1695 (1956).

[5] A. M. Shapiro, Phys. Rev. **84**, 1063 (1951).

[6] Byfield, Kessler, and Lederman, Phys. Rev. **86**, 17 (1952); J. O. Kessler and L. M. Lederman, Phys. Rev. **94**, 689 (1954).

[7] A. E. Ignatenko, *Proceedings of the CERN Symposium* (CERN Organization for Nuclear Research, Geneva, 1956), Vol. II, p. 313; a review of Russian work.

[8] R. H. Miller, Nuovo cimento **6**, 882 (1957).

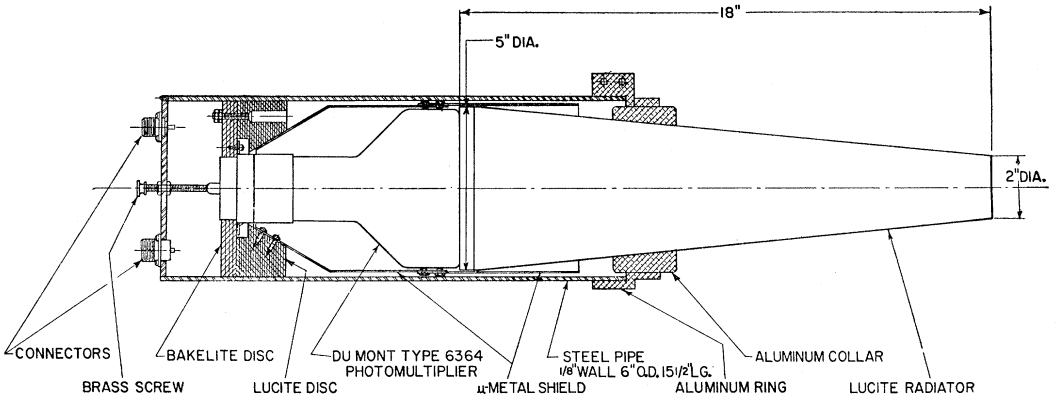

FIG. 2. Side view of the Lucite Čerenkov counter.

cyclotron were brought to the experimental area through a strong-focus magnet and a proper channel in the rotary shield. After momentum analysis by a pion magnet, the beam passed through a steel collimator of 2-in. diam and entered a set of monitor counters No. 1, 2, and 3. Normally a flux of 5×10^5 pions per minute was available for the scattering measurements.

The energy of the incident beam was determined by measuring the range at the position where the scattering targets were placed (45 in. from the exit face of the collimator). The mean range was 70.5 g/cm² in copper, corresponding to the pion energy 150 Mev. The rms spread of the beam was estimated to be ±3 Mev. The fraction of muons and electrons was $(8\pm1)\%$.

The intensity distribution of the beam was surveyed with a $\frac{1}{4}$ in.$\times\frac{1}{4}$ in. traveling counter at the target position. The distribution was approximately Gaussian in both horizontal and vertical directions with a $1/e$ radius of 1 in. The angular spread of the beam was about ±1°. The results were used to obtain an angular resolution width for correcting the elastic cross sections.

Two targets of different thicknesses, one being half the other, were prepared for each element to check the effect of multiple scattering as well as the general consistency of the measurement. They were 1 in. and $\frac{1}{2}$ in. for carbon, $\frac{3}{4}$ in. and $\frac{3}{8}$ in. for aluminum, $\frac{3}{8}$ in. and $\frac{3}{16}$ in. for copper, and $\frac{1}{4}$ in. and $\frac{1}{8}$ in. for lead. Each target was in the form of a 6-in. square and was mounted on a thin aluminum frame. For scattering angles less than 90°, the target was oriented along a bisector of its supplementary angle so that the pion would travel through the same amount of material regardless of its scattering position. For angles larger than 90°, the target was oriented along the bisector of the angle itself to avoid a large amount of energy loss.

Counters No. 1 and 3 were made of a plastic scintillator $2\times2\times\frac{1}{8}$ in. To avoid excessive counting rates in the monitor, counter No. 2 was made of $2\times2\times\frac{3}{8}$ in. Lucite, about one tenth of whose area was spotted by five small disks of plastic scintillators. The ratio of the actual flux entering the target to the monitor rates was frequently calibrated. It was 10.1 ± 0.1 as expected from the fraction of the sensitive area in counter No. 2.

III. DETECTORS

The detector for the present experiment was designed not only to measure the elastic cross section but also to examine the upper part of the energy spectrum of the scattered pions at each angle. For this purpose, the Čerenkov counter was used as an energy spectrometer by analyzing the pulse height of its output.[9] The light output increases with the pion energy if the radiator is long enough to include the full range over which the pions are capable of producing Čerenkov light. The pulse height response of the counter can be calibrated using pions of known energies. Once this calibration has been done, the energy spectrum can be obtained by means of a least-squares analysis from the observed pulse-height distribution for the scattered pions.

A similar procedure can also be used with a large scintillation counter whose sensitive material extends over the full range of the incident pions. While such a counter is expected to produce a greater amount of light output than the Čerenkov counter, it has certain disadvantages for the present purpose: (1) the pulse-height response varies considerably for individual pions due to a large contribution from charged star products when negative pions are captured in the scintillator material, and (2) the large volume required produces many accidental counts in the presence of nucleonic background. In fact, when such a counter was used for negative pions of energy less than 100 Mev, its resolution was 15–20 Mev in comparison with that of the Čerenkov counter 10 Mev at 150 Mev.[8] Thus, for detecting the elastic scattering, the Čerenkov counter is more suitable because of its discrimination against low-velocity particles.

Two Čerenkov counters were constructed for the present experiment. They are called "the Lucite counter" and "the water counter" according to their

[9] Winkler, Mitchell, Anderson, and Peterson, Phys. Rev. **98**, 1411 (1955).

radiator material. A side view of the Lucite counter was shown in Fig. 2. The radiator, of cast Lucite, was tapered into a conical shape from the input end of 2-in. diameter to the output end of 5-in. diameter. This shape served to improve the light collection efficiency by internal reflection. The length of the cone was 18 in., corresponding to the full range over which the pion of 150 Mev can emit Čerenkov light. The output end was viewed by a DuMont 6364 photomultiplier. The photomultiplier and part of the radiator were enclosed in a steel tube and magnetically shielded by a DuMont mu-metal cylinder.

The water counter was constructed in a manner similar to the Lucite counter. The radiator consisted of 17 liters of distilled water with a mixture of DuPont light shifter MDD 3169 (Amino G. Salt)[10] contained in a conical Lucite shell, 14 in. long with an input diameter of $5\frac{1}{8}$ in. and an output diameter of $13\frac{5}{8}$ in. About one third of the output area was viewed by four DuMont 6364 photomultipliers.

As a detector system, a pair of scintillation counters (Nos. 4 and 5 in Fig. 1) were added to each Čerenkov counter. Its functions were to define the solid angle of the system and to provide gating pulses for the pulse-height analyzer. The sizes and positions of these scintillation counters and the amount of tapering of the Čerenkov counter were properly chosen so that most of the scattered pions would not enter or escape from the side-wall of the radiator.

When No. 5 counter was set at 24 in. from the target, the Lucite counter system subtended a solid angle of 0.0055 steradian with an angular half-width of 2.4°. This system was used at the forward angles where a rapid variation of the cross section with the angle was expected. At angles larger than 45° where the amount of scattering decreased considerably, the water counter system was used with a solid angle of 0.12 steradian and an angular half-width of 11.3°.

A block diagram of electronics for the present experiment is shown in Fig. 3. The counting system for the scintillation counters was similar to those already reported in detail by Glicksman, Martin, and Anderson,[11] but a part of the fast coincidence circuit was modified through the introduction of an improved trigger circuit.[12] The resolving time of 3×10^{-8} sec was established by means of clipping lines. The Čerenkov pulses were stretched at the input of the pre-amplifier and split into two branches. In one branch, the pulses were clipped to make a fast coincidence with counters Nos. 1, 3, 4, and 5. In the other, the pulses were shaped to be 1 μsec long and fed through a series of linear amplifiers into a 100-channel pulse-height analyzer.[13] The input

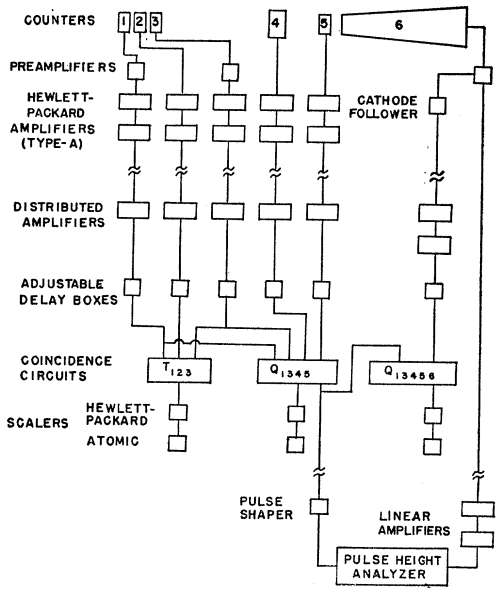

FIG. 3. Block diagram of electronics.

of this analyzer is blocked for $(4N+23)\times10^{-6}$ sec after receiving a pulse in the Nth channel. To avoid a high counting loss, the counting rate was kept less than one pion per cyclotron burst (10^{-4} sec) in the detector systems. The linearity of the amplifier system was checked up to 102 volts at the input of the analyzer. The threshold of the analyzer was set at 12 volts to discriminate against noise pulses from Čerenkov counters.

Three coincidences were set up: the triple T_{123} for monitoring the incident beam, the quadruple Q_{1345} for counting both elastically and inelastically scattered pions above 15 Mev, and the quintuple Q_{13456} for counting those pions which can produce Čerenkov pulses. The quadruple Q_{1345} was also used to gate Čerenkov pulses at the analyzer. An example of the counting rates for scattering from the 1-in. carbon target was given in Table I.

Each detector system was mounted as a unit on a movable cart and set up at the scattering angle within $\pm1°$. A series of target runs and background runs were repeated at least once to check the internal consistency of the data. Whenever a set of scattering measurements was completed at one angle, the detector system was brought back into the incident beam and a calibration procedure (Sec. IV) was made.

IV. CALIBRATION

The pulse-height response of the Čerenkov counter was calibrated for monoenergetic beams of 150±3, 135±4, 120±4, 105±5, and 90±5 Mev. The original beam of 150 Mev was degraded into lower energies by polyethylene stacks placed at the entrance side of the pion magnet. The magnet current was re-adjusted each

[10] E. Heiberg and J. Marshall, Rev. Sci. Instr. **27**, 618 (1956).
[11] Anderson, Glicksman, and Martin, Proc. Nat. Electronics Conf. **9**, 483 (1953).
[12] W. C. Davidon and R. Frank, Rev. Sci. Instr. **27**, 15 (1956).
[13] Model PA-3; Pacific Electro-Nuclear Company, Culver City, California.

TABLE I. Observed counting rates of scattering from ½-in. carbon target. From 18.5° to 43.6°, the solid angle was 5.45×10^{-3} sterad, while from 45° to 139°, the solid angle was 120×10^{-3} sterad.

Angle (deg)	$10^3\times(Q_{1345}/T_{123})_C$	$10^3\times(Q_{1345}/T_{123})_{no}$	$10^3\times(Q_{1345}/T_{123})_{net}$	$10^3\times(Q_{13456}/T_{123})_C$	$10^3\times(Q_{13456}/T_{123})_{no}$	$10^3\times(Q_{13456}/T_{123})_{net}$
18.5	5.014±0.036	1.298±0.018	3.716±0.040	3.427±0.030	0.628±0.013	2.800±0.033
24.3	3.185±0.023	0.756±0.010	2.429±0.025	2.044±0.018	0.255±0.006	1.789±0.019
30.8	1.792±0.021	0.323±0.009	1.470±0.023	1.184±0.017	0.092±0.005	1.092±0.018
36.5	1.151±0.017	0.260±0.009	0.891±0.020	0.631±0.013	0.049±0.003	0.583±0.013
43.6	0.606±0.012	0.135±0.006	0.471±0.013	0.278±0.008	0.019±0.002	0.260±0.008
45	10.480±0.036	1.210±0.014	9.270±0.037	4.805±0.025	0.091±0.004	4.714±0.025
61	4.569±0.027	0.142±0.006	4.427±0.028	0.910±0.012	0.006±0.002	0.904±0.012
75	4.436±0.027	0.072±0.004	4.364±0.027	0.630±0.010	0.005±0.001	0.625±0.010
90	5.486±0.023	0.100±0.003	5.386±0.023	0.715±0.009	0.004±0.001	0.711±0.009
115	5.883±0.031	0.112±0.004	5.771±0.031	0.463±0.009	0.004±0.001	0.459±0.009
139	5.899±0.031	0.172±0.005	5.727±0.031	0.472±0.009	0.006±0.001	0.466±0.009

time to maximize the monitor counts for the beam of the lower momentum. In this way, most of the muons and electrons were removed from the degraded beam.

Typical pulse-height distributions for calibration energies obtained with the Lucite counter are shown in Fig. 4. Each curve was normalized to a fixed number of pions entering the Čerenkov detector. The pulse-height analysis was limited to an effective range of channels between 0 and 80, which corresponded to an input pulse height between 12 and 92 volts. These limits were chosen to eliminate possible distortions due to the noise background and the nonlinearity of the amplifier system. The muons associated with the 150-Mev beam appeared as a separate peak beyond the 80th channel and are not shown in this figure.

The distribution has a peak with a roughly Gaussian shape on which is superimposed a flat tail extending to the lowest pulse height detected. The peak corresponds to pions which travel the full Čerenkov range in the radiator, while the flat tail can be attributed to those which are absorbed or scattered out by the radiator material before they reach the end of the Čerenkov range. For 150 Mev, a ratio of the area under the peak to the total area of the curve was 0.49. This was approximately equal to the attenuation factor resulting from nuclear processes expected for the Lucite counter. A similar agreement was observed for the water counter for which the ratio of the peak to the total area was 0.60.

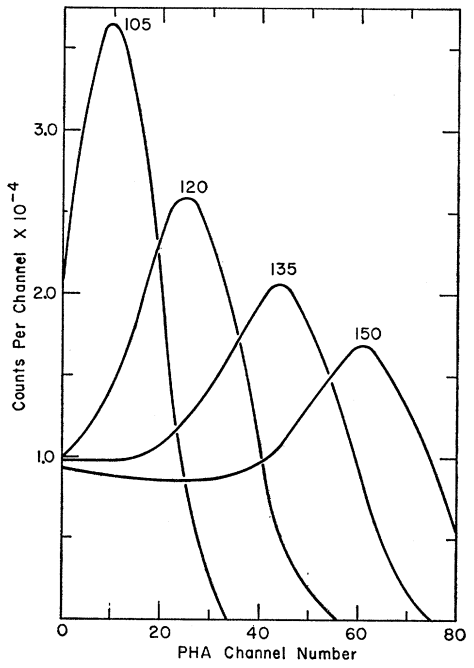

FIG. 4. Smoothed calibration distributions for 4 different monoenergetic pion beams at 150, 135, 120, and 105 Mev, taken with the Lucite Čerenkov counter.

The total number of Čerenkov photons emitted by pions decreases with decreasing pion energy because of the shorter Čerenkov range and the smaller velocity in the radiator. The relation between the peak pulse-height channel and the calibration energy was almost linear as shown in Fig. 5.

The spread of the peak is mainly due to the energy spread of the calibration beam, the straggling in the Čerenkov range, and the statistical fluctuation in the number of photoelectrons of the multiplier. The energy spread and the straggling amounted to about 4 Mev for the 150-Mev pions. The remainder of the observed peak width could be ascribed to the number of photoelectrons if this was taken to be about 100. From the standard formula for Čerenkov emission[14] and the energy loss table, it was possible to estimate that the 150-Mev pions can produce 5000 photons in the spectra range between 3000 A and 5000 A before their velocity is reduced to the threshold of the Lucite radiator ($v/c=0.67$). Thus, the observed width implied that the combined efficiency for light collection and photon-electron conversion was about 2%.

The pulse-height response of the water counter was essentially similar to that of the Lucite counter. The observed peaks were narrower for this counter, indicating a light collection efficiency twice as good as for the Lucite counter.

[14] See, for instance, L. I. Schiff, *Quantum Mechanics* (McGraw-Hill Book Company, Inc., New York, 1949), Sec. 37.

V. DATA ANALYSIS

Figure 6 shows a typical pulse-height distribution of pions scattered at 18.5 from the 1-in. carbon target. The energy response of the Čerenkov counter, while far from ideal, made it possible to deduce the energy spectrum from the observed pulse-height distribution with a reasonable accuracy. The method of analysis is discussed in this section.

Let $K_i(E_\mu)$ be the probability of a pion of energy E_μ being counted in the ith channel of the analyzer. This may be obtained from the calibration distributions as

$$K_i(E_\mu)=N_{i\mu}/N_0,$$

where $N_{i\mu}$ is the number of pulses received in the ith channel when a total number of N_0 of pions of energy E_μ enters the Čerenkov counter. The efficiency of the pulse-height analyzing system is then given by

$$\eta_\mu=\sum_i K_i(E_\mu)=\sum_i N_{i\mu}/N_0,$$

where the index i extends from 1 to 80, the number of channel used. For the Lucite counter, this efficiency varied from 88% for 150 Mev to 40% for 90 Mev. The efficiency decreased with the energy since a larger fraction of pulses were below the threshold of the analyzer for lower energy pions.

Let $q(E)$ be the number of pions leaving a given target with energy E at a given angle. The number of scattered pions counted in the ith channel will be

$$M_i=\int K_i(E)q(E)dE. \quad (1)$$

For practical calculations, the variation of $q(E)$ over an energy interval ΔE may be neglected and the integral can be replaced by a summation over a finite number of energy intervals:

$$M_i=\sum_\mu K_i(E_\mu)q(E_\mu)\Delta E_\mu. \quad (2)$$

Defining a calibration matrix with $A_{i\mu}=K_i(E_\mu)$, Eq. (2) may be written

$$M_i=\sum_\mu A_{i\mu}q(E_\mu)\Delta E_\mu=\sum_\mu A_{i\mu}Q_\mu, \quad (3)$$

where Q_μ is the number of scattered pions in the energy interval of $E_\mu\pm\frac{1}{2}\Delta E_\mu$. In this form, the continuous energy spectrum is approximated by a histogram centered at several calibration energies E_μ.

The least-squares method was used to determine the Q_μ's from the measured M_i's; namely a set of Q_μ's was sought which minimized the quantity,

$$\chi^2=\sum_i\left[\frac{M_i-\sum_\mu A_{i\mu}Q_\mu}{\Delta\nu_i}\right]^2.$$

The value of M_i's was taken to be a difference of the target and the background counts in the ith channel, while the variance of the counts $\Delta\nu_i^2$ was taken to be the sum of the target and the background counts.

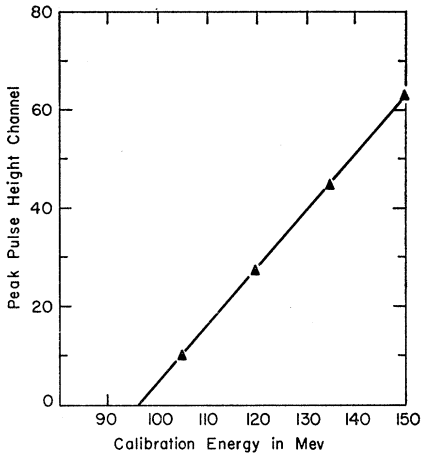

FIG. 5. Channel in which the peak of the calibration distributions appears for various energies of monoenergetic pion beams.

Elements of the calibration matrix A were treated as constants of the analysis since the statistical accuracy of the $A_{i\mu}$'s far exceeds that of the M_i's.

In view of the large amount of scattering data to be analyzed for different angles and targets, the numerical calculation of the least-squares analysis was programmed for AVIDAC, the electronic computer at the Argonne National Laboratory. The code was prepared by R. H. Miller of this laboratory. For a given set of input data M_i, $\Delta\nu_i^2$, and $A_{i\mu}$, the code was capable of evaluating Q_μ's corresponding to a minimum χ^2. In addition, the error matrix associated with these Q_μ's was calculated so that the mean square errors in the

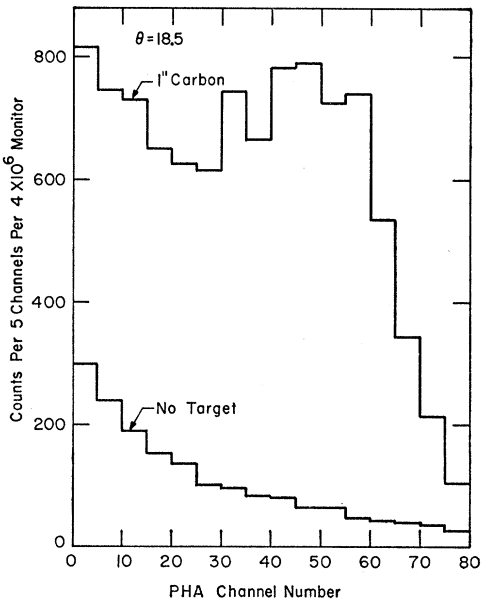

FIG. 6. Pulse-height spectrum of pions scattered from the 1-in. target at 18.5°, measured with the Lucite Čerenkov counter. The counts are summed in each 5 channels. The background is also shown.

TABLE II. Counts per 15 Mev reduced by energy analysis for 1-in. carbon target at 18.5°.

Energy	150 Mev	135 Mev	120 Mev	105 Mev	90 Mev
Q_μ	535	1819	−77	221	26
Error matrix	908	−764	178	−121	16
		2388	−1330	384	−287
			1918	−1033	515
				1511	−990
					1536

Q_μ's as well as their correlation coefficients were made available.

The number of energy intervals into which the pulse height distribution can be analyzed was inherently limited by the resolution of the counter. After several trials, the optimum number was chosen for each counter so that the error matrix could properly be obtained from the analysis. The data taken with the Lucite counter were analyzed in terms of five calibration energies with an energy interval of $\Delta E_\mu = 15$ Mev. A typical result of the analysis is given in Table II for the scattering data at 18.5° from the 1-in. carbon target. Although Q_μ is essentially a positive quantity, the analyses occasionally give negative results. These could be taken to be zero within their statistical errors. A re-analysis with such Q_μ's forced to zero produced no substantial change in the other Q_μ's.

In the analysis of the water counter data, a standard function was deduced which fit the measured calibration distributions. This function had the form

$$A_{i\mu} = A_\mu F(n_i - n_\mu),$$

where A_μ is a normalizing coefficient, n_i a variable channel number, and n_μ the peak channel number which corresponds to the pion energy E_μ. The function $F(n_i - n_\mu)$ represented a Gaussian with a 10-channel peak width for $n_i \geq n_\mu$, with a flat tail of height corresponding to $\frac{1}{5}$ of the peak height added for $n_i < n_\mu$. All water counter data were analyzed in terms of six calibration distributions having their peak at $n_\mu = 70$, 55, 40, 25, 10, and −5. During each scattering run, a new calibration measurement was obtained which served to establish an energy corresponding to each peak channel. In this way, the effect of the gain drifts of the photomultiplier was taken into account.

Once the Q's were determined by the energy analysis, the differential cross section for the scattered pions with energy $E \pm \frac{1}{2}\Delta E$ at a given angle was calculated by the following formula:

$$\frac{d^2\sigma}{d\Omega dE} = \frac{Q_\mu \cos(\theta/2)}{N\Delta\Omega f_\pi f_a R_m \epsilon T_{123}} = B_0 \frac{Q_\mu}{T_{123}}, \tag{4}$$

where Q_μ/T_{123} is the ratio of the number of scattered pions with energy $E_\mu \pm \frac{1}{2}\Delta E_\mu$ to the triple rates of the incident beam monitor. The solid angle subtended by the detector system at the center of the target is represented by $\Delta\Omega$: $(5.45 \pm 0.11) \times 10^{-3}$ steradian for the Lucite counter and $(1.20 \pm 0.02) \times 10^{-1}$ steradian for the water counter. The number of target nuclei per cm² is N. The factor $\cos(\theta/2)$ takes into account the effective increase of N due to the particular orientation of the target described in Sec. II. This was replaced by $\sin(\theta/2)$ for angles larger than 90°. The fraction f_π of pions in the beam was 0.92 ± 0.01. The quantity f_a corrects for the attenuation of the incident beam in the target. The average attenuation varied from 2% to 4%, depending on the target and the angles. The ratio R_m of the true counts at the target to the monitor counts was 10.1 ± 0.1, as already described in Sec. II. A further correction was made for the attenuation of the scattered beam between target and the Čerenkov counter. The fraction of pions which decayed in flight before reaching the Čerenkov counter was calculated, using the pion mean life 2.92×10^{-8} sec. This varied between 4% and 5.5% for the energies between 150 and 90 Mev when the Lucite counter was used. The corresponding variation was between 2% and 3% for the water counter, which was operated at a shorter distance from the target. In addition, 5% of the scattered pions were absorbed or scattered out by the gating counters Nos. 4 and 5. These losses were

TABLE III. $d^2\sigma/d\Omega dE$ in mb per steradian per 15 Mev for carbon.

Target	Angle \ Energy (Mev)	150	135	120	105	90
1 in. C	18.5°	63.8± 5.0	231 ±14	9.2± 5.3	26.6± 1.5	3.1± 4.8
½ in. C		109 ±10	164 ±15	7.6±11	40.3±10.5	3.6±10.8
1 in. C	24.3°	47.3± 3.2	127 ± 8	2.8± 2.7	16.0± 3.5	2.5± 2.5
½ in. C		109 ± 8	77.4± 7.8	3.7± 6.6	5.9± 5.0	7.0± 5.5
1 in. C	30.8°	26.8± 2.5	80.3± 5.5	4.8± 2.9	13.1± 2.6	1.2± 2.5
½ in. C		44.7± 3.7	55.7± 5.1	4.1± 3.5	13.4± 3.4	0.1± 3.6
1 in. C	36.5°	4.9± 0.9	48.5± 3.5	1.6± 2.2	0.7± 2.2	1.3± 2.2
½ in. C		20.0± 2.5	26.2± 3.7	5.5± 3.1	2.1± 3.0	7.3± 3.6
1 in. C	43.6°	1.9± 1.4	15.2± 1.5	3.1± 1.3	3.6± 1.3	5.4± 0.7
½ in. C		7.5± 1.4	8.3± 1.9	7.0± 1.9	0.9± 1.9	5.3± 2.1

TABLE IV. $d^2\sigma/d\Omega dE$ in mb per steradian per 15 Mev for aluminum.

Target	Angle \ Energy (Mev)	150	135	120	105	90
$\frac{3}{4}$ in. Al	18.5°	118 ± 9	423 ±25	23 ± 9	43 ± 9	35 ± 9
$\frac{3}{8}$ in. Al		271 ±19	303 ±24	14 ±15	44 ±14	44 ±15
$\frac{3}{4}$ in. Al	24.3°	56 ± 5	204 ±12	3 ± 4	30 ± 5	7 ± 4
$\frac{3}{8}$ in. Al		156 ±12	106 ±12	4 ± 8	24 ± 9	6 ±10
$\frac{3}{4}$ in. Al	30.8°	15 ± 2	81 ± 6	3 ± 4	15 ± 3	1 ± 3
$\frac{3}{8}$ in. Al		49 ± 5	51 ± 6	7 ± 6	14 ± 6	9 ± 6
$\frac{3}{4}$ in. Al	36.5°	3.3± 1.3	19.8± 4.3	9.5± 2.5	2.0± 2.6	9.1± 3.2
$\frac{3}{8}$ in. Al		8.9± 2.7	18.8± 4.1	6.8± 3.8	0.9± 4.3	6.2± 5.2
$\frac{3}{4}$ in. Al	43.6°	1.0± 0.9	10.2± 1.7	4.1± 1.8	3.9± 2.0	7.5± 2.5
$\frac{3}{8}$ in. Al		2.8± 1.5	5.8± 2.2	4.3± 2.3	6.7± 2.9	0.8± 3.1

taken into account by the factor ϵ. All nonstatistical quantities in the cross section formula were collected in the coefficient B_0.

The error estimate for $d^2\sigma/d\Omega dE$ was complicated by the fact that the values of the Q_μ's were correlated. The uncertainties in B_0 and T_{123} had to be combined with the errors in the Q_μ's through an error matrix. For practical purposes, the statistical error in T_{123} could be neglected and the value of B_0 could be taken to be constant over various energy channels. The error matrix for a set of $d^2\sigma/d\Omega dE$ at a given angle from a given target was given by

$$\frac{1}{T_{123}^2}[B_0^2\Delta_{\mu\nu}+(\Delta B_0)^2Q_\mu Q_\nu], \tag{5}$$

where $\Delta_{\mu\nu}$ is the error matrix associated with Q_μ. The systematic error $\Delta B_0/B_0$ was of the order of 5% for all angles and targets.

VI. EXPERIMENTAL RESULTS

The energy-dependent cross sections, $d^2\sigma/d\Omega dE$, obtained at angles less than 45° for carbon, aluminum, copper, and lead are summarized in Tables III, IV, V, and VI, respectively. The error shown for each cross section was determined from the diagonal element of the error matrix as given by (5). The energies listed are those of the scattered pions coming out of the target. Because of the difference in the ionization loss, the value of $d^2\sigma/d\Omega dE$ for the full-thickness target is not necessarily equal to the corresponding value for the half-thickness target. At angles less than 45°, the energy loss due to ionization in the full-thickness target was about 10 Mev, while the loss due to nuclear recoil was negligibly small (less than 1 Mev). Thus, the histogram representation of the energy spectrum obtained with the full-thickness target differs by 5 Mev in energy from that obtained with the half-thickness target.

A general feature of the energy spectrum can be seen in a plot of all values of $d^2\sigma/d\Omega dE$ as a function of energy. Figure 7 shows an example of such a plot for carbon at 18.5°. In this figure, the difference in the energy loss between the 1-in. and $\frac{1}{2}$-in. targets was already taken into account. If a reasonably smooth curve is drawn through all measured points, the spectrum indicates a distinct peak centered at 140 Mev and a small amount of inelastic scattering below 120 Mev. The full width of the peak at half maximum was about 20 Mev as expected from the counter resolution. A

TABLE V. $d^2\sigma/d\Omega dE$ in mb per steradian per 15 Mev for copper.

Target	Angle \ Energy (Mev)	150	135	120	105	90
$\frac{3}{8}$ in. Cu	18.5°	60 ±12	804 ±50	278 ±17	128 ±24	175 ±26
$\frac{3}{16}$ in. Cu		335 ±24	690 ±38	104 ±23	178 ±22	127 ±22
$\frac{3}{8}$ in. Cu	24.3°	36 ± 6	253 ±17	30 ± 9	42 ± 9	66 ±10
$\frac{3}{16}$ in. Cu		97 ±11	144 ±15	12 ±12	75 ±12	4 ±14
$\frac{3}{8}$ in. Cu	30.8°	6.1± 2.4	45 ± 5	17.5± 5.0	18.7± 5.6	44.2± 7.1
$\frac{3}{16}$ in. Cu		17.5± 5.0	34 ± 7	9.3± 6.3	22.0± 6.7	18.7± 8.8
$\frac{3}{8}$ in. Cu	36.5°	1.2± 1.9	31.1± 3.6	16.5± 3.9	14.0± 4.5	15.2± 5.2
$\frac{3}{16}$ in. Cu		9.0± 3.6	34.4± 6.0	13.2± 5.8	14.1± 6.9	5.3± 8.3
$\frac{3}{8}$ in. Cu	43.6°	1.9± 1.8	31.9± 4.0	4.4± 3.5	9.9± 3.8	8.1± 4.0
$\frac{3}{16}$ in. Cu		6.1± 2.6	27.0± 4.8	5.3± 4.5	0.9± 4.5	18.9± 5.6

TABLE VI. $d^2\sigma/d\Omega dE$ in mb per steradian per 15 Mev for lead.

Target	Angle \ Energy (Mev)	150	135	120	105	90
$\frac{1}{4}$ in. Pb	18.5°	1070±87	2085±144	891±100	978±100	842±106
$\frac{1}{8}$ in. Pb		872±77	1400±166	739± 95	997±115	732±110
$\frac{1}{4}$ in. Pb	24.3°	258±25	395± 37	256± 34	317± 37	347± 42
$\frac{1}{8}$ in. Pb		237±34	227± 43	104± 40	272± 48	230± 57
$\frac{1}{4}$ in. Pb	30.8°	74±12	163± 20	76± 19	158± 23	164± 27
$\frac{1}{8}$ in. Pb		124±20	126± 26	55± 14	79± 33	166± 36
$\frac{1}{4}$ in. Pb	36.5°	6± 7	91± 13	50± 14	70± 16	118± 21
$\frac{1}{8}$ in. Pb		6±12	58± 18	57± 19	27± 23	56± 30
$\frac{1}{4}$ in. Pb	43.6°	7± 5	33± 9	23± 9	20± 11	57± 15
$\frac{1}{8}$ in. Pb		31±10	7± 12	33± 12	10± 15	46± 19

similar behavior was observed for the scattering at the forward angles from aluminum, copper, and lead. The separation between the peak and the inelastic continuum, however, became less distinct for heavier elements and at the larger angles. In Fig. 7, the peaks of the energy spectra for carbon at 24.3°, 30.8°, 36.5°, and 43.6° are illustrated on the same scale for comparison.

The energy spectra obtained with the water counter for carbon at angles larger than 45° are shown in Fig. 8. A distinct peak was still present at 45° but diminished quite rapidly with increasing angle. At 60°, the peak became broader and most of the scattering appeared to be inelastic. The spectrum at 115° was almost flat in the energy region above 120 Mev. This is typical for the spectra of both carbon and lead obtained at angles larger than 90°.

The elastic scattering cross section was determined from $d^2\sigma/d\Omega dE$ in the energy intervals where the distinct peak appeared. At large angles where the peak was not clearly distinguished, the energy intervals where the elastic scattering should be split by the analysis were identified by the energy of the elastically scattered pions at these angles (e.g., 132 Mev at 115°). The results are given in Table VII.

The term "elastic," in the strict sense, applies only to the scattering in which the nucleus is left in the original state. The measured elastic scattering cross sections, however, possibly include some amount of inelastic scattering with energy loss less than the half-width of the peak (10 Mev). Such an inelastic contribution may come from those pions which have excited the nucleus to nearby levels or ejected a nucleon from the nucleus. If the contribution from the excited levels were a substantial fraction of the elastic scattering cross section, this would broaden the lower side of the elastic peak. In the case of carbon, such an effect was not apparent in the energy spectrum at angles less than 45°. To verify this point, an independent check was made as follows. A monoenergetic pulse-height distribution was calculated by the standard function (Sec. V) with its peak corresponding to the energy of the elastic pions at the given angle. By an energy analysis of this distribution, the relative number of the elastically scattered pions which fell into each energy interval could be determined. At 45°, the relative values of this number were in agreement with the $d^2\sigma/d\Omega dE$'s obtained from the scattering measurement within their experimental accuracy. This indicates that no large contribution came from the excited levels of carbon at angles less than 45°. Recently, Baker has roughly measured the cross sections for scattering of 80-Mev pions from the excited levels of carbon with an improved differential range method.[15] He found that the contribution from these levels became comparable with the elastic scattering cross section at angles larger than 90°. If it is assumed, according to Baker, that the relative amount of inelastic scattering depends mainly on the momentum transfer of the pions, we would expect a large inelastic contribution at angles larger than 56° for the present energy. This is consistent with our observation of the broadened peak at angles larger than 60°. The experimental results for electron scattering[16]

TABLE VII. Elastic scattering cross sections of 150-Mev pions, in mb per steradian.

Angle	Carbon	Aluminum	Copper	Lead
18.5°	295 ±17	551 ±32	957 ±80	2270 ±140
24.3°	178 ±10	260 ±15	272 ±16	583 ± 90
30.8°	104 ± 6	98 ± 7	51.2± 4.1	241 ± 18
36.5°	50.6 ± 3.3	24.5± 2.2	35.5± 5.5	78 ± 16
43.6°	16.0 ± 1.3	10.2± 1.1	33.5± 3.1	36 ± 6
44.8°	15.1 ± 1.5			29.0± 3.0
61.0°	2.4 ± 0.3			9.2± 1.7
74.8°	1.2 ± 0.2			2.8± 0.8
90.1°	0.52± 0.07			2.9± 0.7
115.0°	0.78± 0.07			2.4± 0.7
138.6°	0.38± 0.07			1.6± 0.8

[15] W. F. Baker, Columbia University Nevis Cyclotron Laboratories Report, NEVIS-48, 1957 (unpublished).

[16] R. Hofstadter, Revs. Modern Phys. **28**, 214 (1956); J. H. Fregeau, Phys. Rev. **104**, 225 (1956).

and proton scattering[17] also suggest no large inelastic scattering from the excited levels at forward angles.

The inelastic continuum observed below 120 Mev could be ascribed to the process in which the pions were encountered by individual nucleons. Because of the continuous nature of the spectrum, it is possible that some fraction of this process was included within the experimental elastic energy width. The inelastic contribution of this type was estimated on the basis of Monte Carlo calculations,[18] which were originally carried out for the analysis of the inelastic scattering data at 150 Mev.[8] The result of this correction will be discussed in Sec. VIII.

Besides the inelastic scattering, the following effects were considered which may give a spurious contribution to the elastic cross sections. (a) The multiple Coulomb scattering of the incident beam from the target may increase the elastic scattering cross section at small angles. (b) Muons which arise from decay in flight of pions may travel with a slight angle to the incident beam (the maximum angle is 9° for the present beam). Some of these muons may be scattered into the detector and produce a pulse in the same channels as the elastically scattered pions. (c) Neutral pions produced by the charge exchange scattering of negative pions decay promptly into two gamma rays, part of which can in turn be converted into a pair of electrons inside the target. Since the radiators of both Čerenkov counters were about one radiation length, there is a finite probability of these electrons contributing to $d^2\sigma/d\Omega dE$ in the high-energy intervals.

The effects of (a) and (b) were appreciably large (5 and 10%, respectively) only at 18.5° for the $\frac{1}{4}$-in. lead target. Hence, the elastic scattering cross section of lead at this angle was determined from the measurement with the $\frac{1}{8}$-in. target alone. The contribution from muons which came through the pion magnet was automatically rejected by the pulse-height analysis because of their high velocity.

The effect of (c) was estimated in the order of magnitude by using the total charge exchange cross section of 100 mb for lead as measured by Lederman *et al.*[6] and the electron range in the radiator calculated by Wilson's Monte Carlo method.[19] Simplified assumptions were made concerning the angular and energy distributions for neutral pions and electrons. The estimated contribution of 3 mb per steradian per 15 Mev was consistent with the observed $d^2\sigma/d\Omega dE$ in the highest energy intervals of the spectra at backward angles. The correction for the other targets were negligible.

[17] K. Strauch and F. Titus, Phys. Rev. **103**, 200 (1956); **104**, 191 (1956).

[18] Bivins, Metropolis, Storm, Turkevich, Miller, and Friedlander, Bull. Am. Phys. Soc. Ser. II, **2**, 63 (1957). The writer is indebted to Dr. N. Metropolis, Dr. M. Storm, Dr. R. Bivins, and Dr. A. Turkevich for their kindly providing the results of Monte Carlo calculations conducted on the MANIAC electronic computer at the Los Alamos Scientific Laboratory.

[19] R. R. Wilson, Phys. Rev. **84**, 100 (1952).

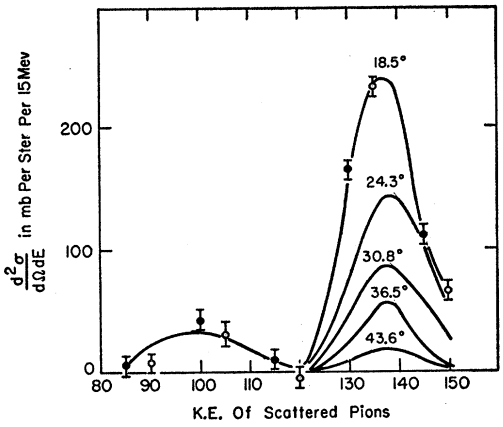

FIG. 7. Energy spectra of pions scattered from carbon, as measured with the Lucite Čerenkov counter. Open circles are the 1-in. target points and closed circles are the $\frac{1}{2}$-in. target points at 18.5°. For the energy spectra at 24.5°, 30.8°, 36.5°, and 43.6°, only the height of the elastic peaks are shown on the same scale. The experimental elastic energy is 140 Mev. The ordinate is in mb per steradian per 15 Mev.

VII. OPTICAL MODEL CALCULATION

The optical model treats the nucleus as an optical medium with a complex index of refraction. This medium changes the phases and attenuates the amplitude of a plane wave of the incident particles. The wave inside the nucleus can be described by a solution of the wave equation with a complex potential. By matching appropriate conditions at the nuclear bound-

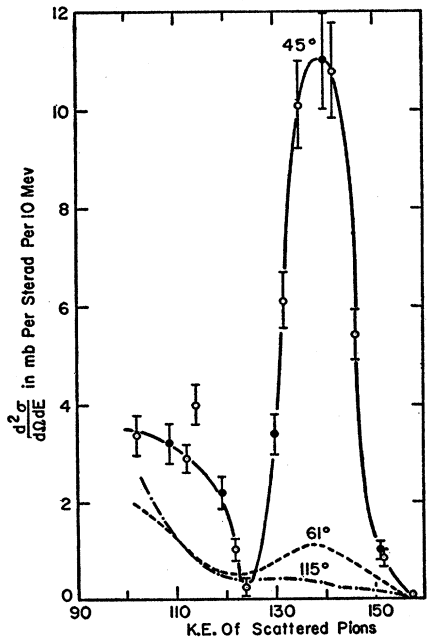

FIG. 8. Energy spectra of pions scattered from carbon at 45°, 61°, and 115°, as measured with the water Čerenkov counter. The experimental points are shown only for 45°; the open circles are for the 1-in. target and closed circles are for the $\frac{1}{2}$-in. target. The ordinate is in mb per steradian per 10 Mev.

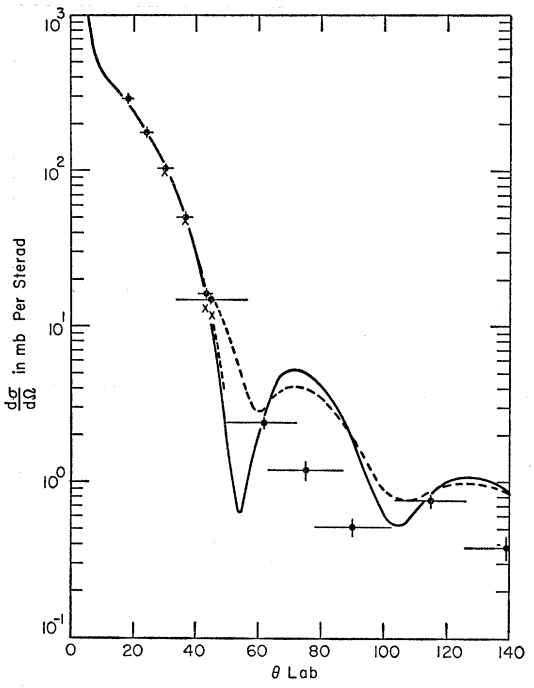

FIG. 9. Angular distribution for elastic scattering of 150-Mev negative pions by carbon. The solid curve is the optical model calculation with parameters $r_0=1.4\times10^{-13}$ cm, $V_R=-40$ Mev, and $V_I=-65$ Mev. The broken curve is the calculation folded into the angular resolution. The closed circles are the measured elastic scattering cross sections. The crosses are the cross sections after subtraction of the inelastic contributions.

ary, the equation can be solved to provide the differential cross section for the coherent scattering and the total reaction cross section. The latter includes all incoherent processes such as absorption, inelastic scattering, and charge-exchange scattering in the case of the pion-nucleus interaction.

The model has been widely used in the analysis of the scattering data for proton,[20] neutron,[21] and alpha-particle scattering[22] since the original application by Fernbach, Serber, and Taylor.[23] The procedure of the analysis for the present experiment was similar to those adopted for the earlier experiments on pion-nucleus scattering.[4,7] A brief description will be given.

The Klein-Gordon equation for a pion of total energy E,

$$\nabla^2\psi+\frac{(E-V)^2-\mu^2c^4}{\hbar^2c^2}\psi=0, \tag{6}$$

can be solved by a partial wave method:

$$\psi(r,\theta)=\sum_l \frac{u_l(r)}{r}Y_l^0(\theta).$$

The radial wave function of angular momentum l satisfies the equation

$$\frac{d^2u_l}{dx^2}-\frac{l(l+1)}{x^2}u_l+\left(1-\frac{2EV}{p^2c^2}+\frac{V^2}{p^2c^2}\right)u_l=0, \tag{7}$$

where $x=kr$ and k and p are the wave number and the momentum of the incident pion, respectively.

Within a nucleus of radius $R=r_0A^{\frac{1}{3}}$, the potential was assumed to be $V=V_R+iV_I$. The equation for the inside solution has the form

$$\left[\frac{d^2}{dx^2}-\frac{l(l+1)}{x^2}+a+ib\right]u_l=0, \tag{8}$$

where

$$\begin{aligned}a&=1-(2EV_R-V_R^2+V_I^2)/p^2c^2,\\ b&=2V_I(V_R-E)/p^2c^2.\end{aligned} \tag{9}$$

In analogy to the optics, the complex index of refraction n is given by $n^2=a+ib$ and nk represents the wave number of the pion inside the nucleus. Since the reaction mean free path λ_t is related to the imaginary part of the index of refraction by $n=n_0+i/2K\lambda_t$,[24] λ_t is in turn related to V_R and V_I through parameters a and b by

$$\lambda_t=\frac{1}{K}\{2[(a^2+b^2)^{\frac{1}{2}}-a]\}^{-\frac{1}{2}}=\frac{\hbar}{\mu c}\frac{1}{\eta}\{2[(a^2+b^2)^{\frac{1}{2}}-a]\}^{-\frac{1}{2}}. \tag{10}$$

This can be reduced to the nonrelativistic formula $\lambda_t=\hbar v/2V_I$ for $V\ll E$.[3]

Outside the nuclear radius ($r\geq R$), the potential was taken to be the attractive Coulomb potential $V=-Ze^2/r$. The equation for the outside region is

$$\left[\frac{d^2}{dx^2}-\frac{l(l+1)}{x^2}+1-\frac{2\eta_c}{x}\right]u_l=0, \tag{11}$$

where $\eta_c=-Ze^2/\hbar v$ and the V^2 term was neglected.[25]

The inside solution for the lth partial wave can be given by a spherical Bessel function of the lth order, while the outside solution by a linear combination of regular and irregular Coulomb functions.[26] The phase shift δ_l is determined by matching the logarithmic derivative of both solutions at the nuclear boundary.

[20] See, for instance, Melkanoff, Nodvik, Saxon, and Wood, Phys. Rev. **106**, 793 (1957).

[21] See, for instance, Eisberg, Gugelot, and Porter, Brookhaven National Laboratory Report BNL-331(C-21), 1955 (unpublished); T. B. Taylor, Ph.D. thesis, Cornell University, 1954 (unpublished).

[22] See, for instance, G. Igo and R. M. Thaler, Phys. Rev. **106**, 126 (1957).

[23] Fernbach, Serber, and Taylor, Phys. Rev. **75**, 1352 (1949).

[24] See, for instance, N. C. Francis and K. M. Watson, Am. J. Phys. **21**, 659 (1953),

[25] At the nuclear surface $R=(\hbar/\mu c)\times A^{\frac{1}{3}}$, the Coulomb potential is of the order of $Z/A^{\frac{1}{3}}$ Mev. This is much smaller than the total energy $E=239$ Mev.

[26] Reference 14, Sec. 20.

The scattering amplitude for the outgoing wave is

$$f(\theta)=f_C(\theta)+\frac{1}{K}\sum_l(2l+1)e^{2i\sigma_l+i\delta_l}\sin\delta_l P_l(\cos\theta),$$

where $f_C(\theta)$ is the pure Coulomb amplitude

$$f_C(\theta)=-\frac{\eta_c}{1-\cos\theta}\exp[-i\eta_C l_n(1-\cos\theta)+i2\sigma_0],$$

and

$$\sigma_l=\mathrm{Arg}(1+l+i\eta_C).$$

The numerical computations of this partial wave method were performed on the AVIDAC at the Argonne National Laboratory. A code which was originally prepared for proton-nucleus scattering by Solmitz was modified for the present purpose.[27] The input for the calculation consists of the wave number of the incident pions k, the nuclear radius R, the potential parameters a and b, the Coulomb parameter η_c, and the maximum angular momentum number L. A typical value for these parameters are listed in Table VII. The value of L was taken large enough to include any significant contribution from the higher partial waves. The code was capable of calculating the differential cross sections at two-degree steps between 2° and 136° as well as the total reaction cross section with a rounding error of 0.1 mb. An average time required for one set of calculations was about 1.5 minutes.

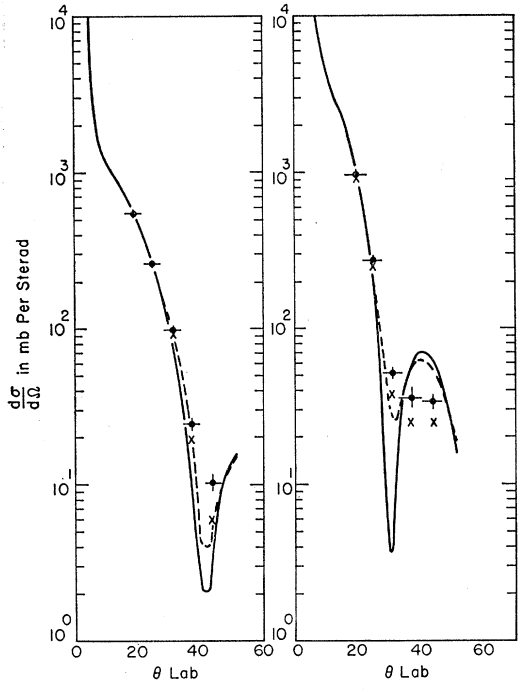

FIG. 10. FIG. 11.

FIG. 10. Angular distribution for elastic scattering by aluminum. The parameters are $r_0=1.4\times10^{-13}$ cm, $V_R=-30$ Mev, and $V_I=-65$ Mev. The description is the same as in Fig. 9.

FIG. 11. Angular distribution for elastic scattering by copper. The parameters are $r_0=1.4\times10^{-13}$ cm, $V_R=-30$ Mev, and $V_I=-75$ Mev. The description is the same as in Fig. 9.

[27] F. T. Solmitz (private communication).

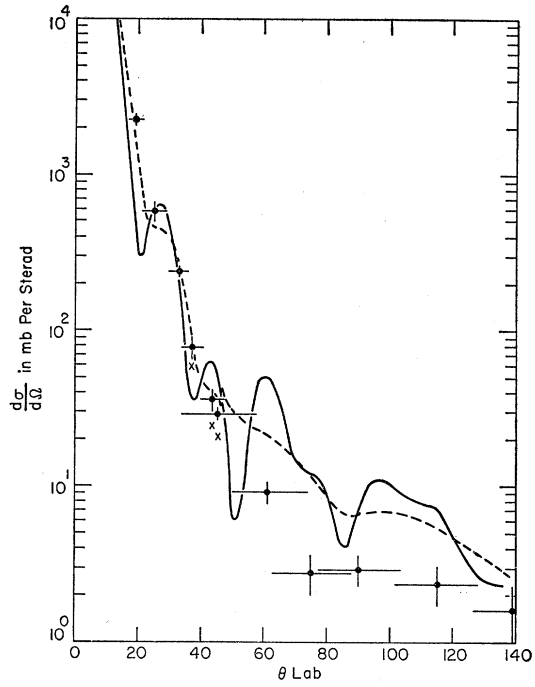

FIG. 12. Angular distribution for elastic scattering by lead. The parameters are $r_0=1.4\times10^{-13}$ cm, $V_R=-30$ Mev, and $V_I=-65$ Mev. The description is the same as in Fig. 9.

VIII. COMPARISON

The angular distributions of elastic scattering from carbon, aluminum, copper, and lead are illustrated in Figs. 9, 10, 11, and 12 respectively. In each figure, a solid curve represents the result of the optical model calculation which was carried out with parameters listed in Table VII. The measured cross sections are plotted with closed circles. The experimental error and the angular resolution width are shown at each point. The broken curve and crosses in each figure will be described later in this section.

The calculated angular distribution shows an oscillating diffraction pattern with sharp minima and maxima, which are the characteristic features for the square well model. The minima occur at angles which are close to these predicted by the modified Born approximation formula,[4]

$$2n_0kR\sin(\theta/2)=4.49,\ 7.73,\ \cdots \text{ etc.},$$

where R is the nuclear radius, k the wave number of the pion, and n_0 the real part of the index of refraction (Sec. VII). Since the wave number inside the nucleus, n_0k, is increased by the presence of the attractive potential V_R, the minima shift to smaller angles for the larger negative value of V_R assumed in the calcu-

lation. For carbon, aluminum, and copper, the calculated curve starts to rise steeply as the angle decreases below 10°, where Coulomb scattering overtakes diffraction scattering. In the case of lead, the effect of the Coulomb potential is dominant in the angular range below 45°. This was borne out by comparing the results of two calculations, one with the nuclear potential alone and the other with both nuclear and Coulomb potentials.

For a comparison with the experimental results, the calculated curves were modified to take into account the finite angular resolution of the detector. The broken curve in each figure shows the result of folding the original distribution (the solid curve) with an angular resolution function, which includes the effects of the finite extention of the detector, the beam distribution at the target, and the multiple scattering in the target. With the Lucite detector, the effect was small (2–5%) for carbon, but it was appreciably near the diffraction minima for aluminum, copper, and lead. The large angular width of the water detector (12°) suppressed the diffraction pattern at the large angles.

The measured cross sections (closed circles) include presumably some amount of inelastic scattering as discussed in Sec. VI. The inelastic contribution estimated on the basis of Monte Carlo calculation was subtracted from the measured cross section at each angle less than 45°. The results are plotted with crosses in Figs. 9, 10, 11, and 12. This subtraction process was not meaningful at angles larger than 60° since the correction became of order comparable to the measured cross section. At these angles, however, the measurement has already indicated much less elastic scattering (by a factor of 2 to 5) than any of the square well calculations predicts. This is in contrast to the results of the earlier experiments in which a slight rise of the elastic scattering cross sections above the calculated values was observed at the backward angles.[4,6] Such large cross sections in the earlier experiments were possibly due to the inelastic scattering against which the present experiment was able to discriminate better. This was confirmed by the recent results of Baker, who

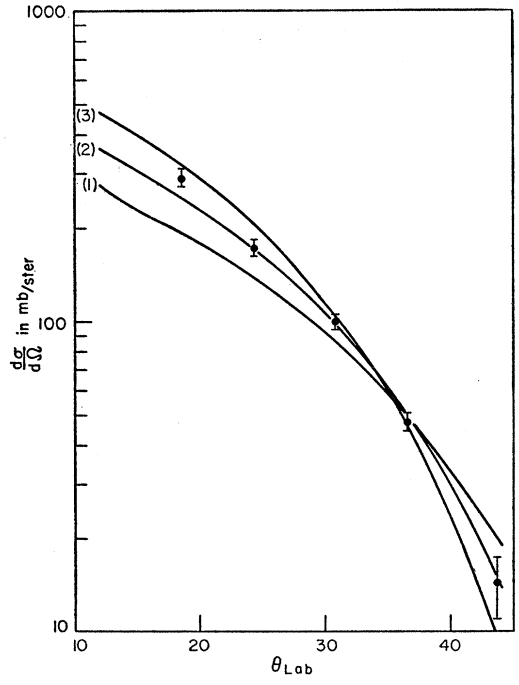

FIG. 13. Variation of angular distribution of carbon for three different radii. $V_R=-40$ Mev and $V_I=-55$ Mev. (1) $r_0=1.3\times10^{-13}$ cm, (2) $r_0=1.4\times10^{-13}$ cm, and (3) $r_0=1.5\times10^{-13}$ cm. The angular resolution is folded into all calculations shown here. The experimental values are corrected for the inelastic contributions.

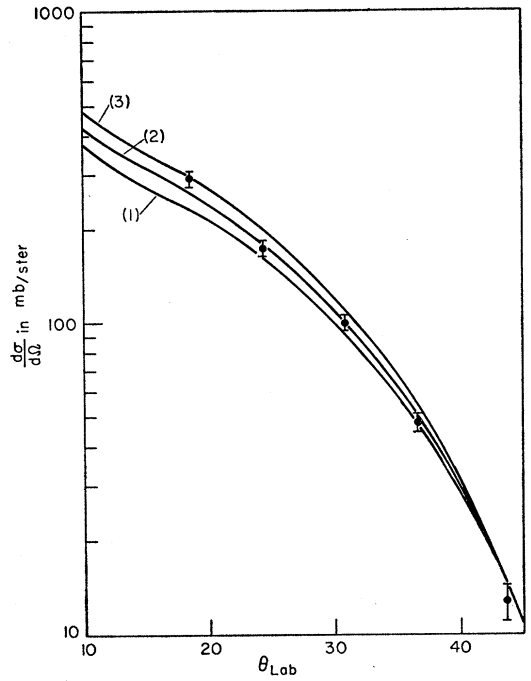

FIG. 14. Variation of angular distribution of carbon for three different real potentials: (1) $V_R=-30$ Mev, (2) $V_R=-40$ Mev, and (3) $V_R=-50$ Mev with $r_0=1.4\times10^{-13}$ cm and $V_I=-65$ Mev. The description is the same as in Fig. 13.

repeated the measurement at 80 Mev with the improved energy resolution.[15] He found that the cross sections at large angles were reduced by a factor of 2 to 10 from the old values.

By comparing the calculated curves and the experimental results (Figs. 9–12), it is evident that any qualitative fit can be expected only over the angular region below 45°. The calculation could be improved at large angles by modifying the square well shape, such as the surface term suggested by Kisslinger[28] or the diffuse-edge potential initiated by Saxon and Woods.[29] In either case, an additional parameter is required

[28] L. S. Kisslinger, Phys. Rev. **98**, 761 (1955).
[29] R. D. Woods and D. S. Saxon, Phys. Rev. **95**, 577 (1954).

which depends on the surface condition of the nuclear matter. In view of the uncertainties involved in the large-angle cross sections, such an extra effort in the calculation would not be justified for the present purpose.

The three optical-model parameters, r_0, V_R, and V_I, were varied to see their individual effects on the forward angular distributions. The effect of varying r_0 is illustrated in Fig. 13 for carbon. The experimental points could be fitted quite well by the curve calculated with $r_0=1.4\times10^{-13}$ cm. Figures 14 and 15 show the effects of varying V_R and V_I for carbon and aluminum, respectively. The angular distribution is more sensitive to the value of V_R at the smaller angles, while the

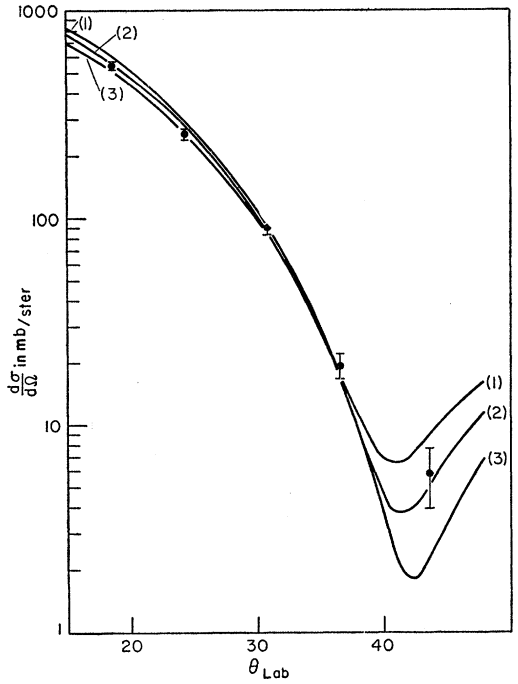

FIG. 15. Variation of angular distribution of aluminum for three different imaginary potentials: (1) $V_I=-85$ Mev, (2) $V_I=-65$ Mev, and (3) $V_I=-45$ Mev with $r_0=1.4\times10^{-13}$ cm and $V_R=-30$ Mev. The description is the same as in Fig. 13.

variation of V_I produces little effect except near the diffraction minimum.

An attempt was made to determine the best-fit values of r_0, V_R, and V_I by the least-squares method. Namely, those values of parameters were sought which minimized

$$\chi^2=\sum_i\left[\frac{\sigma_E(\theta_i)-\sigma_c(\theta_i)}{\delta_i}\right]^2.$$

At each angle θ_i, $\sigma_E(\theta_i)$ is the experimental cross section, δ_i the error attached to $\sigma_E(\theta_i)$, and $\sigma_c(\theta_i)$ the calculated cross section. The variation of the χ^2 value was examined in a two dimensional potential space for the few fixed values of r_0. Figure 16 illustrates such a plot for

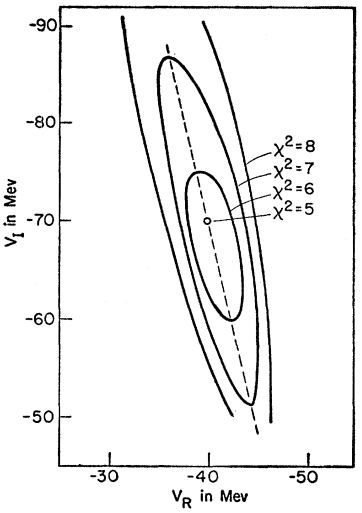

FIG. 16. Variation of the χ^2 value for carbon data in the V_R-V_I plane. The radius parameter is $r_0=1.4\times10^{-13}$ cm.

the carbon data with $r_0=1.4\times10^{-13}$ cm. The minimum of the χ^2 value (5) was located at $V_R=-40$ Mev and $V_I=-70$ Mev. No better fit was obtained with $r_0=1.3\times10^{-13}$ cm nor with 1.5×10^{-13} cm. A similar but less extensive search was done for heavier elements. A broad minimum of the χ^2 value was found at $V_R=-28$ Mev and $V_I=-64$ Mev with $r_0=1.4\times10^{-13}$ cm for aluminum, and at $V_R=-30$ Mev and $V_I=-75$ Mev with $r_0=1.3\times10^{-13}$ cm for copper.

The errors associated with these parameters may come from several sources: the standard deviations in the least-squares analysis, the uncertainties in the corrections applied to the cross sections, and a particular choice of the angular range (less than 45°). The accurate estimate of each effect was difficult. However, taking all effects into consideration, a reasonable estimate would be ±6 Mev for V_R and ±10 Mev for V_I with the carbon data, and twice as much for aluminum and copper. More confidence can be attached to the carbon data than to the heavier nuclei since (1) the angular distribution is most sensitive to the variation of parameters for carbon and (2) both angular and inelastic corrections were smallest for carbon. In view of these uncertainties, one can choose the ranges of the best-fit parameters for the present results as $V_R=-30$ to -40 Mev, $V_I=-65$ to -75 Mev, and $r_0=(1.3$ to $1.4)\times10^{-13}$ cm. The corresponding mean free path can be calculated by Eq. (10). It was of the order of the pion Compton wavelength, $(1.2$ to $1.4)\times10^{-13}$ cm.

There was a difficulty in obtaining a good fit to the experimental data of lead even in the angular range below 45°. The value of χ^2 was quite large (30–40) and did not vary significantly in the wide range of parameters: $V_R=0$ to -45 Mev, $V_I=-45$ to -85 Mev, and $r_0=(1.0$ to $1.4)\times10^{-13}$ cm. The measurement indicated a smoother variation of cross sections than any calculated curves (Fig. 12). This trend may be accounted for by using the diffused edge model as has been done

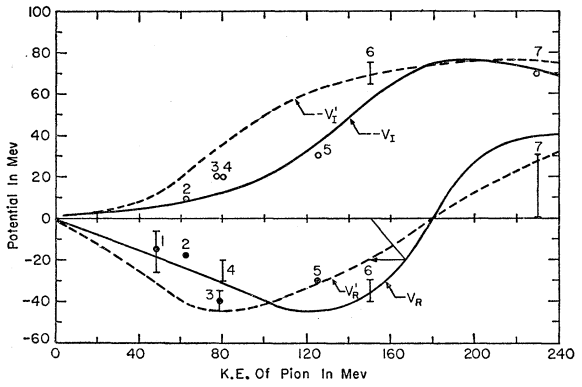

FIG. 17. Energy dependence of optical model potential. The solid curves are the theoretical values calculated by FGW (reference 3). They are replotted as a function of the incident energy (broken curves). The experimental points labeled 1–7 are described in Sec. IX.

by Woods and Saxon.[29] In the angular range below 25°, Coulomb interference seems to play a major role. The calculated angular distribution also depends on the charge distribution inside the nucleus. A simple cutoff of the point-charge Coulomb potential at the nuclear boundary, which was assumed in the present calculations, may not be adequate for the heavy nucleus.[16] Whatever model be chosen, however, the present result could hardly be a sensitive test because of the large size of the lead nucleus.

Besides the elastic scattering angular distributions, the total reaction cross sections of carbon and lead were obtained by subtracting the elastic scattering part from the attenuation cross section. The attenuation cross sections were determined by a transmission measurement in a manner as described by Miller.[8] The results are compared with the values calculated for the parameters which provided the best fit to the angular distribution of carbon in Table VIII. The observed reaction cross section for carbon is larger than the calculated value by $1\frac{1}{2}$ standard deviations. The calculated cross section varies only as much as ± 10 mb within the uncertainties in V_R and V_I. Thus, the observed reactions cross section of carbon seems to indicate a slightly longer radius parameter ($r_0=1.45\times10^{-13}$ cm) than the value which gives the best fit to the forward angular distribution of elastic scattering ($r_0=1.40\times10^{-13}$ cm). The experimental cross section of lead is in agreement with the values calculated with $r_0=1.40\times10^{-13}$ cm.

In comparison with the experimental results obtained at 125 Mev by Kessler and Lederman[6] and at 135 Mev by Martin,[30] the present value of the reaction cross section for carbon is larger but the total attenuation cross section is comparable. This is due to the small amount of large-angle elastic scattering found in the present experiment. Indeed, the sum of the elastic and inelastic differential cross sections at large angles is in good agreement with that of Kessler and Lederman's data, as has been already pointed out by Miller.[8]

[30] R. L. Martin, Phys. Rev. **87**, 1052 (1952).

IX. DISCUSSION

In analogy to the classical dispersion theory, the optical model potential can be related to the properties of nuclear constituents by[31]

$$V(w)=-\frac{2\pi\hbar^2c^2}{E}\rho_n f_0(w),$$

where E is the total energy of the incident pion, ρ_n the nucleon density of the nucleus, f_0 the forward scattering amplitude for pion-nucleon scattering averaged over protons and neutrons in the nucleus, and w the energy at which scattering takes place inside the nucleus. This relation leads to the possibility of calculating V from the pion-nucleon scattering data. The basic assumption required is that f_0 for free pion-nucleon scattering would not be modified appreciably in the presence of many-body forces inside the nucleus.

The simplest approach to the problem is to use directly the values of f_0 obtained in pion-nucleon scattering at the similar energy. This neglects several effects due to nuclear binding, such as the momentum distribution of nucleons and the correlation in nucleon positions.[3] The real part of f_0 can be calculated from a set of pion-nucleon phase shifts, while the imaginary part is related, via $I_m(f_0)=k/4\pi\sigma_{\text{total}}$, to the total cross sections for π^++p and π^-+p scattering. Recently, Frank, Gammel, and Watson[3] have improved such a "free-particle calculation" in several aspects; (1) the values of $R_e(f_0)$ were used which were determined directly from the total cross sections by the principle of causality,[32] (2) a correction due to the Pauli exclusion principle was applied to reduce the free pion-nucleon cross section in calculating $I_m(f_0)$, and (3) an absorption term was included in the imaginary part of V. The absorption cross section of the nucleus was obtained by $\sigma_a(\text{nucleus})=\Gamma\sigma(\pi^++d\rightarrow p+p)$, where Γ takes into account the probability of forming a quasi-deuteron state in the nucleus.

The theoretical values of V_R and V_I thus calculated from the pion-nucleon interaction are shown by solid curves in Fig. 17. They are given as a function of the kinetic energy of the pion "inside the nucleus" by the original authors.[3] In order to compare with the experimental results, however, it is more convenient to replot both curves as functions of the incident energy of the pion. This can be done by converting the variable of the abscissa according to an equation $E_{\text{incident}}=E_{\text{inside}}-V_R$. The result of such a conversion is shown by broken curves. The results of the present and earlier experiments are labeled as follows: 1, π^- of energy 48

[31] The relativistic equation was used with the approximation $V\ll E$.

[32] Anderson, Davidon, and Kruse, Phys. Rev. **100**, 358 (1955).

Mev for carbon by Shapiro[5]; 2, π^- of 62 Mev for carbon by Byfield *et al.*[6]; 3, $\pi^\pm$ of 78 Mev for copper by Williams *et al.*[4]; 4, $\pi^\pm$ of 80 Mev for aluminum by Pevsner *et al.*[4]; 5, π^- of 125 Mev for carbon and lead by Kessler *et al.*[6]; 6, the present experiment, and 7, π^- of 230 Mev for carbon by Dzelepov *et al.*[7] For the experiments labeled 2, 5, and 7 the value of V_I was calculated from the quoted value of the mean free path λ_t using Eq. (10).

The value obtained for V_I in the present experiment agrees well with the theoretical value, indicating the influence of strong $\pi^+ + p$ ($\pi^- + n$) scattering near the resonance energy. This is in contrast to some results at the lower energies, where a smaller imaginary potential (longer mean free path) has been given by the experiment. The real potential at the present energy was found to be attractive as predicted, but somewhat deeper than the calculated value. A similar result ($V_R = -24 \pm 6$ Mev) has been obtained from the recent emulsion work on the energy spectrum of inelastic scattering at 160 Mev.[33] The qualitative disagreement in V_R would not be too surprising in view of the assumptions made in the model of Frank, Gammel, and Watson. In particular near the resonance energy, the short mean free path increases the uncertainty in the pion energy between scatterings with nucleons inside the nucleus. This would make it less valid to use the forward scattering amplitude on the energy shell for calculating V_R.[3] The effect of correlation in nucleon positions inside the nucleus may also serve to increase the value of V_R.[2,3]

It is interesting to note that Russian cloud chamber work has recently suggested the possibility of V_R being positive at 230 Mev.[7] This is, when taken together with the present result, indicative of a change in sign for V_R in the pion energy between 180 and 200 Mev. In view of the large uncertainty involved in the experimental determination of the potentials, a further evidence on the positive V_R above 200 Mev would be desirable to confirm the characteristic features the calculation by Frank, Gammel, and Watson.

[33] Nikol'skii, Kudrin, and Ali-Zade, J. Exptl. Theoret. Phys. U.S.S.R. **32**, 48 (1957) [translation: Soviet Phys. JETP **5**, 93 (1957)].

TABLE VIII. Typical values of parameters used for the calculation.

Element	r_0 (10^{-13} cm)	V_R (Mev)	V_I (Mev)	$-Ze^2/\hbar v$	kR	L
Carbon	1.4	−40	−65	0.050	4.12	7
Aluminum	1.4	−30	−65	0.108	5.40	8
Copper	1.4	−30	−75	0.242	7.19	10
Lead	1.4	−30	−65	0.683	10.65	13

X. ACKNOWLEDGMENTS

The writer is greatly indebted to Professor Herbert L. Anderson, who suggested this problem, for his guidance and encouragement throughout the work. He is also grateful to Professor S. Courtenay Wright who followed the work and generously gave advice and assistance. Thanks are due to Dr. F. Solmitz for making available his code for the optical model calculations, and to Dr. W. C. Davidon and Dr. D. Flanders of the Argonne National Laboratory for their help with the AVIDAC computations. The assistance of Mr. J. F. Fainberg during the course of the experiment is gratefully acknowledged. Finally, the writer would like to express his gratitude to Dr. R. H. Miller, whose active cooperation through all stages of the work made the task easier.